SYNAPSE 61:595–605 (2007)

Kinetic Evaluation in Nonhuman Primates of Two New PET Ligands for Peripheral Benzodiazepine Receptors in Brain

MASAO IMAIZUMI, EMMANUELLE BRIARD, SAMI S. ZOGHBI, JONATHAN P. GOURLEY, JINSOO HONG, JOHN L. MUSACHIO, ROBERT GLADDING, VICTOR W. PIKE, ROBERT B. INNIS, AND MASAHIRO FUJITA*

Molecular Imaging Branch, National Institute of Mental Health, National Institutes of Health, Bethesda, Maryland

KEY WORDS arterial input function; aryloxyanilide; compartmental modeling; distribution volume; positron emission tomography

ABSTRACT Peripheral benzodiazepine receptors (PBRs) are upregulated on activated microglia and are, thereby, biomarkers of cellular inflammation in brain. We recently developed two PET ligands with an aryloxyanilide structure to image PBRs and now evaluate the kinetics of these radiotracers in monkey to determine whether they are suitable to explore in human. Baseline and receptor-blocking scans were performed with [^{11}C]PBR01 and [^{18}F]PBR06 in conjunction with serial measurements of the arterial plasma concentration of parent radiotracer separated from radiometabolite. We used brain and plasma data with compartmental modeling to calculate regional brain distribution volume, which is equal to the ratio at equilibrium of the concentration of radioligand in brain to that of plasma. The distribution volume of [^{11}C]PBR01 was inaccurately estimated in the baseline scans, possibly because of the short half-life of ^{11}C or the presence of radiometabolite in brain. In contrast, the distribution volume of [^{18}F]PBR06 was stably determined within 200 min of scanning, and nondisplaceable uptake was only ~10% of total brain uptake. [^{18}F]PBR06 is promising for use in human because brain activity could be quantified with standard compartmental models and showed higher ratios (~10:1) of specific to nonspecific uptake. A critical factor for human use will be whether the tracer has adequately fast wash out from brain relative to the half-life of the radionuclide to obtain stable values of distribution volume. **Synapse 61:595–605, 2007.** Published 2007 Wiley-Liss, Inc.†

INTRODUCTION

The peripheral benzodiazepine receptor (PBR) was initially discovered in peripheral organs (and thus its name) but was later found in the central nervous system. In all organs, PBR is a protein located on the mitochondrial outer membrane and a member of a trimeric complex with adenosine nucleotide translocase and the voltage-dependent anion channel (McEnery et al., 1992). Although the physiological role of PBR is unclear, it has been implicated in various functions, including neurosteroid synthesis (Papadopoulos et al., 1997), immunomodulation (Zavala, 1997), cell proliferation (Okuyama et al., 1999; Schlichter et al., 2000), and apoptosis (Bono et al., 1999). In normal brain, PBRs are found primarily in glial cells, with especially high densities in olfactory bulb, choroid plexus, and the ependymal lining of the ventricles (Anholt et al., 1984; Benavides et al., 1983; Cymerman et al., 1986; Schoemaker et al., 1983). PBR expression is markedly increased in activated microglia and reactive astrocytes (Banati, 2002, 2003), which are found following neuronal damage and in several neurodegenerative diseases (Benavides et al., 1987; Cagnin et al., 2002). For this reason, positron emission tomography (PET) imaging of PBRs has been used as a biomarker for neuroinflammation. The most widely used selective ligand is (*R*)-*N*-[^{11}C]methyl-*N*-(methylpropyl)-1-(2-chlorophenyl)-isoquinoline-3-carboxamide ([^{11}C](*R*)-PK 11195). Brain uptake of [^{11}C](*R*)-PK 11195 is increased in several disorders, including Alzheimer's (Cagnin et al., 2001a; Groom

Contract grant sponsor: Intramural Research Program of the National Institute of Mental Health; Contract grant number: #Z01-MH-002795-04.

*Correspondence to: Masahiro Fujita; Molecular Imaging Branch, National Institute of Mental Health, National Institutes of Health Building 31, Room B2B37, 31 Center Drive, MSC 2035, Bethesda, Maryland 20892-2035, USA. E-mail: fujitam@mail.nih.gov

Received 12 October 2006; Accepted 29 December 2006

DOI 10.1002/syn.20394

Published online in Wiley InterScience (www.interscience.wiley.com).

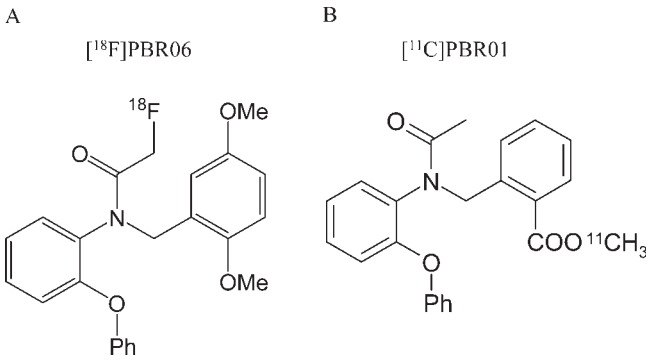

Fig. 1. Structures of [^{18}F]PBR06 and [^{11}C]PBR01.

et al., 1995) and Parkinson's diseases (Ouchi et al., 2005), multiple sclerosis (Banati et al., 2000; Debruyne et al., 2003), stroke (Price et al., 2006), Rasmussen's encephalitis (Banati et al., 1999), herpes encephalitis (Cagnin et al., 2001b), amyotrophic lateral sclerosis (Turner et al., 2004), and multiple system atrophy (Gerhard et al., 2003). However, a low ratio of specific to nonspecific binding may limit its sensitivity to detect therapeutic interventions. Its relatively high lipophilicity ($c\log P = 5.3$) may have caused high nonspecific binding in brain (Petit-Taboue et al., 1991).

More promising PET tracers for PBR have recently been developed and have an aryloxyanilide structure (Okuyama et al., 1999). *N*-([^{11}C](2,5-dimethoxybenzyl)-*N*-(5-fluoro-2-phenoxyphenyl)acetamide ([^{11}C]DAA1106) and *N*-(5-fluoro-2-phenoxyphenyl)-*N*-(2-^{18}F-fluoroethyl-5-methoxybenzyl)acetamide ([^{18}F]FEDAA1106) have successfully imaged PBRs in human and nonhuman primates with high brain uptake and a high percentage of specific binding (Fujimura et al., 2006; Maeda et al., 2004; Zhang et al., 2003).

We synthesized two aryloxyanilide compounds that have high affinity and selectivity for PBRs: ([^{18}F]PBR06 and [^{11}C]PBR01) (Briard et al., 2005a,b) (Fig. 1). The objective of this study was to assess the utility of these two PET radioligands to quantify PBRs in monkey brain. Using compartmental methods of measuring brain uptake relative to plasma levels of the radioligand, we found that *N*-[^{18}F]-fluoroacetyl-*N*-(2,5dimethoxybenzyl)-2-phenoxyaniline ([^{18}F]PBR06) provided accurate estimates of PBR densities with high levels of specific biding and, therefore, is suitable for exploratory studies in human subjects.

MATERIALS AND METHODS

Synthesis of radioligands

PBR06 was labeled by treatment of the bromo precursor with cyclotron-produced [^{18}F] fluoride ion. Experimental labeling proceeded in almost quantitative radiochemical yield (Briard et al., 2005b) (Fig. 1A).

Okubo et al. reported that methyl 2-((*N*-(2-phenoxyphenyl)-acetamido)-methyl)benzoate has high binding affinity for PBR (Okubo et al., 2004). We also prepared this ligand and its parent carboxylic acid. Treatment of the acid with [^{11}C]methyl iodide gave [methyl-^{11}C]methyl 2-((*N*-(2-phenoxyphenyl)-acetamido)-methyl)benzoate ([^{11}C]PBR01) (Fig. 1B) in good radiochemical yield for evaluation with PET (Briard et al., 2005a).

The specific radioactivity of [^{18}F]PBR06 and [^{11}C]PBR01 at the injection was 26.8 ± 17.5 and 71.5 ± 37.2 GBq/μmol with these and subsequent data expressed as mean ± SD, respectively (Table I).

In vitro receptor-binding assays

Following the previously described procedures (Chaki et al., 1999), we measured the binding affinity (K_i) of PBR06, PBR01, and PK11195 to displace [^{3}H]PK 11195 binding to monkey brain mitochondrial preparations. K_i values for each test compound were calculated according to the equation of Cheng and Prusoff (Cheng and Prusoff, 1973), using the K_D (dissociation constant of the tritiated radioligand) value obtained from Scatchard analysis.

The NIMH Psychoactive Drug Screening Program measured the affinity of PBR06 to a large number of receptors and transporters that are listed in Results section. Detailed receptor-binding protocols are available at their web site (http://pdsp.med.unc.edu).

PET scans

All animal experiments were performed in accordance with the Guide for the Care and Use of Laboratory Animals and were approved by the NIMH Animal Care and Use Committee. We used three rhesus monkeys (*Macacca mulatta*, body weight: 12.8 ± 2.5 kg) (Table I). Anesthesia was initiated with i.m. injection of ketamine (10 mg/kg) and then maintained with 1.6% isoflurane and 98.4% O_2. Electrocardiograph, body temperature, heart, and respiration rates were measured throughout the experiment. Body temperature was maintained at 37.0–37.5°C.

We used two PET scanners for this study. The GE Advance device (General Electric Medical Systems, Waukesha, WI) has a reconstructed resolution of 7.5-mm full-width half-maximum in all directions in 3D mode. The High Resolution Research Tomograph (HRRT; Siemens/CPS, Knoxville, TN, USA) device has a reconstructed resolution of 2.5-mm full-width half-maximum in all directions in 3D mode. After the radiopharmaceutical was injected intravenously, coronal slices covering the whole brain were obtained. PET scans were acquired for 90–300 min (33–60 frames with scan duration ranging from 30 s to 5 min). Blocking experiments used either nonradioactive PBR01 (1 mg/kg) or DAA1106 (3 mg/kg), administered at the same time (PBR01), or 24-min prior (DAA1106) to the radiotracer administration (Table I). DAA1106 was used to block

TABLE I. List of nonhuman primate [^{11}C]PBR01 and [^{18}F]PBR06 PET imaging

PET Ligand	Scan No.	PET	Scan length (h)	Animal No.	Blocking agent	Blocking dose (mg/kg)	Specific activity (GBq/mmol)	Injected activity (MBq)
[^{18}F]PBR06	1 Baseline	GE Advance	2	1	–	–	22	215
	2 Blocking	GE Advance	2	1	DAA 1106	3.0	16	188
	3 Baseline	HRRT	5	2	–	–	53	139
	4 Baseline	HRRT	5	3	–	–	16	102
[^{11}C]PBR01	5 Baseline	GE Advance	2.5	3	–	–	21	137
	6 Blocking	GE Advance	1.5	3	PBR01	1.0	110	105
	7 Baseline	HRRT	3	2	–	–	76	175
	8 Blocking	HRRT	1.5	2	PBR01	1.0	80	182

[^{18}F]PBR06 binding because nonradiolabeled PBR06 was not available and the kinetics of DAA1106 is slow enough to block the binding throughout the experiment (Maeda et al., 2004).

Measurement of radiotracer concentration in plasma

Details of the measurement are as described previously (Zoghbi et al., 2006). The plasma time-activity curve was corrected by the amount of unchanged radioligand in plasma. For this purpose, blood samples (0.5 mL each) were drawn at 15-s intervals until 2 min, followed by 1-mL samples at 3, 5, 10, 30, 60, 90, and 120 min. Each blood sample was immediately put in heparinized tubes and then separated into plasma and blood cell fraction by centrifugation. Plasma samples (450 μL) were mixed with acetonitrile (700 μL) containing reference PBR06 or PBR01. Distilled water (100 μL) was added and mixed well. Total radioactivity in this solution was measured with a calibrated gamma counter. Deproteinized plasma samples were centrifuged at 10,000*g* for 1 min to remove denatured proteins. The supernatant was then analyzed directly by reversed phase high-performance liquid chromatography (HPLC) on Novapak C18 (Waters, Milford, MA) with a radial compression module RCM-100, eluted with MeOH:H_2O:Et_3N (75:25:0.1 by vol. and 80:20:0.1 by vol. for [^{18}F]PBR06 and [^{11}C]PBR01, respectively) at 2.0 mL/min. The percent recovery of radioactivity in the supernatant from each sample was calculated relative to that in the precipitate, which was 91.6 ± 2.4% ($n = 64$) for [^{18}F]PBR06 and 91.6 ± 1.2% ($n = 58$) for [^{11}C]PBR01, respectively. The efficiency of recoveries of plasma standards that were constructed by adding a known amount of parent radioactivity and subjected to the same analytical steps as each plasma sample resulted in an efficiency of 97.0 ± 0.7% ($n = 4$) and 96.2 ± 1.6% ($n = 4$) for [^{18}F]PBR06 and [^{11}C]PBR01, respectively.

Image analysis

The tomographic images were analyzed with PMOD 2.65 (pixel-wise modeling computer software; PMOD Technologies, Adliswil, Switzerland) (Burger et al., 1998). A summed image from all frames was coregistered to a T1-weighted magnetic resonance (MR) image acquired separately on a GE 1.5 T Signa MR scanner (SPGR, TR/TE/flip angle = 13.1 ms/5.8 ms/45°, 0.4 × 0.4 × 1.5 mm^3 with coronal acquisition on a 256 × 256 × 60 matrix) (GE Medical Systems, Waukesha, WI) using Statistical Parametric Mapping (SPM) 2 (Wellcome Department of Cognitive Neurology, London, UK). Regions of interest (ROIs) were defined on the MR image for the frontal (volume: 222 mm^3), temporal (364 mm^3), parietal (234 mm^3), and occipital (194 mm^3) cortices, cerebellum (1,043 mm^3), putamen (164 mm^3), thalamus (129 mm^3), and choroid plexus of fourth ventricle (81 mm^3). To normalize brain uptake relative to injection activity and the body weight, standardized uptake values (%SUV) were calculated as (% injected activity/cm^3 brain) × body weight (g).

Estimation of distribution volume with arterial input function

Time-activity data were analyzed with both one- and two-tissue compartment models (Cunningham, 1995), using the radiometabolite-corrected plasma input function. Rate constants (K_1, k_2, k_3, and k_4) were estimated with weighted least squares and the Marquardt optimizer. Brain date of each frame was weighed based on the noise equivalent counts.

In the one-tissue compartment model, K_1 and k_2 are the rate constants governing the transfer of the ligands in and out of the brain, respectively. In the two-tissue compartment model, K_1 and k_2 are the rate constants governing the transfer of the ligands in and out of the nondisplaceable compartment, whereas k_3 and k_4 describe the rate of association and dissociation to and from the receptor, respectively.

For the one-tissue compartment model,

$$V = K_1/k_2$$

where V is the distribution volume for the single tissue compartment.

For the two-tissue compartment model,

$$V = K_1/k_2(1 + k_3/k_4).$$

Nonlinear least-squares analysis was performed with PMOD 2.65 (Burger et al., 1998).

Statistical analysis

Goodness-of-fit by nonlinear least squares analysis was evaluated using the Akaike information criterion (AIC) (Akaike, 1974) and model selection criterion (MSC).

AIC is calculated by the following formula,

$$\mathrm{AIC} = n\mathrm{In}\left(\sum_{i=1}^{n} w_i(Y_{\mathrm{obs}_i} - Y_{\mathrm{cal}_i})^2\right) + 2p$$

MSC is calculated by the following formula,

$$\mathrm{MSC} = \mathrm{In}\left(\frac{\sum_{i=1}^{n} w_i(Y_{\mathrm{obs}_i} - \overline{Y}_{\mathrm{obs}})^2}{\sum_{i=1}^{n} w_i(Y_{\mathrm{obs}_i} - Y_{\mathrm{cal}_i})^2}\right) - 2p/n$$

where n is the number of data points, w_i is the weights applied to the points, p is the number of parameters, Y_{cal_i} is the value calculated by a model, and Y_{obs_i} is the observed data in an experiment.

MSC is a modification of the AIC. The most appropriate model is that with the *smallest* AIC value and the *largest* MSC value. MSC was proposed by Micromath Scientific Software (Salt Lake City, Utah) and implemented in their program, "Scientist."

Goodness-of-fit by one- and two-tissue compartment models was compared with F statistics (Hawkins et al., 1986). A value of $P < 0.05$ was considered significant for F statistics.

The standard error of nonlinear least squares estimation for rate constants was given by the diagonal of the covariance matrix (Carson, 1986) and expressed as a percentage of the rate constants (coefficient of variation, %COV). In addition, %COV of distribution volume (V) was calculated from the covariance matrix using the generalized form of error propagation equation (Bevington and Robinson, 2003), where correlations among parameters were taken into account.

RESULTS

Binding characteristics for two aryloxyanilides

PBR06 and PBR01 potently displaced [^{3}H]PK 11195 binding to crude mitochondrial preparations of monkey brain. The K_i values of both compounds were similar (PBR06; $K_i = 0.30 \pm 0.08$ nM and PBR01; $K_i = 0.24 \pm 0.04$ nM) and of higher affinity than PK 11195 ($K_i = 3.48 \pm 1.26$ nM; mean ± SD from six separate measurements).

The selectivity of PBR06 was screened at a large number of receptors and transporters. PBR06 (10 μM) caused less than 50% displacement of specific binding at the following receptors: serotonin $5HT_{1a}$, $5HT_{1b}$, $5HT_{1d}$, $5HT_{1e}$, $5HT_{2a}$, $5HT_{2b}$, $5HT_{2c}$, $5HT_3$, $5HT_{5a}$, $5HT_6$, $5HT_7$, adrenergic α_{1a}, α_{1b}, α_{2a}, α_{2b}, α_{2c}, β_1, β_2, β_3, dopamine D_1, D_2, D_3, D_4, histamine H_1, H_2, H_3, H_4, muscarinic cholinergic M_2, M_5, $GABA_A$ receptors composed of $\alpha_1\beta_1\gamma_2$, $\alpha_2\beta_2\gamma_2$, $\alpha_5\beta_2\gamma_2$, and $\alpha_6\beta_2\gamma_2$ subunits; dopamine, norepinephrine, and serotonin transporters.

Pharmacological effects in nonhuman primates

A total of eight PET scans were performed in three monkeys (Table I). In these PET scans, the injected mass dose of [^{18}F]PBR06 and [^{11}C]PBR01 was 0.22 ± 0.11 and 0.11 ± 0.11 μg/kg, respectively. In all baseline and blocking experiments using DAA1106 (3 mg/kg) and nonradiolabeled PBR01 (1 mg/kg), the differences between pre- and postinjection vital signs were: <15 mm Hg for systemic blood pressure, <10/min for pulse, <5/min for respiratory rate, and <0.3°C for temperature.

Plasma analysis

After injection of both [^{18}F]PBR06 and [^{11}C]PBR01, plasma activity of unchanged radioligands peaked at ~2 min and decreased quickly thereafter (Figs. 2C and 3C). The radioactive metabolites increased at late time points to 70–80% of total plasma activity. The HPLC retention time for radioactive metabolites and plasma parent were 2.47 ± 0.18 and 6.64 ± 0.25 min for PBR06 ($N = 63$), and 2.47 ± 0.19 and 5.56 ± 0.38 ($N = 55$) min for PBR01, respectively, indicating that the metabolites were less lipophilic than the parent compounds.

The concentration of parent radiotracer in plasma markedly increased after administration of the receptor-blocking agent. For example, the concentration of [^{18}F]PBR06 at 5 min increased from 26 to 101% SUV after DAA1106 (3 mg/kg i.v., before radioligand injection; Fig. 2C and 2D). Similarly, the concentration of [^{11}C]PBR01 at 5 min increased from 24 to 115% SUV after PBR01 (1 mg/kg i.v. administered with the radioligand; Fig. 3C and 3D). PBRs are found in high density in peripheral organs such as lung and kidney (Anholt et al., 1986). Receptor-saturating doses of the nonradioactive ligands likely increased the plasma concentration of radiotracer by blocking these peripheral sites.

Distribution and blockade of brain uptake

In baseline experiments, both radioligands showed high peak brain uptake (300% SUV) and a widespread distribution, with greater activity in gray than in white matter (Fig. 4). The choroid plexus in the fourth ventricle had highest levels of activities at late time points (Fig. 4), consistent with the known distribution of PBRs.

In blocking experiments, brain activity at early time points was increased because of elevated plasma concentrations of radiotracer, as described earlier. For example, the peak uptake of [^{18}F]PBR06 was ~300% SUV at baseline and ~800% SUV after receptor blockade (Fig. 2A and 2B). Similarly, the peak uptake of

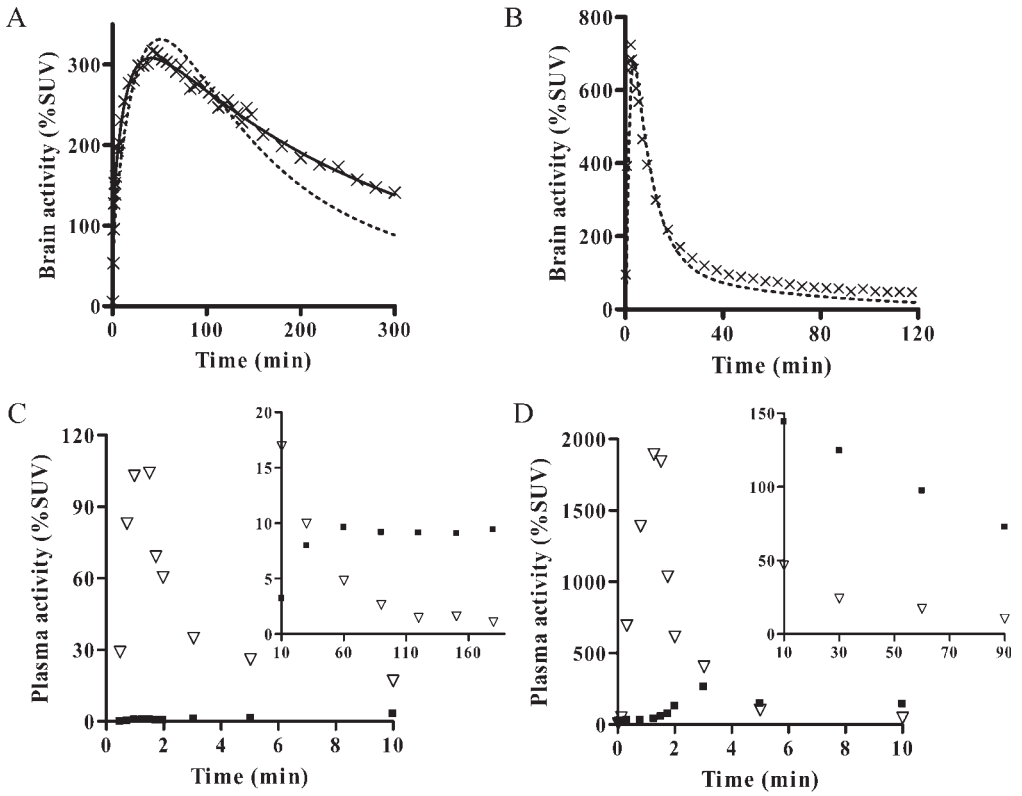

Fig. 2. Representative [^{18}F]PBR06 brain time-activity curves, compartmental fittings, and radioligand concentrations in plasma at baseline (**A** and **C**; scan #4, Table I) and after receptor blockade (**B** and **D**; scan #2, Table I). The aryloxyanilide derivative DAA1106 (3 mg/kg i.v.) was injected 24 min before [^{18}F]PBR06 in the blocking experiment. In the brain curves (A and B), the dashed line is the one-tissue compartment fitting, and the solid line is the two-tissue compartment fit. The two-tissue compartmental fitting did not converge in the blocking scan (B). For the plasma curves (C and D), the inset graphs show the lower plasma activities after 10 min. Symbols: (×) putamen, (▽) plasma parent, and (■) major radiometabolite.

[^{11}C]PBR01 was ~300% SUV at baseline and ~600% SUV after receptor blockade (Fig. 3A and 3B). Both [^{18}F]PBR06 and [^{11}C]PBR01 showed average regional activity washout rates (percentage decreases from peak uptake times to 120 min) of 18–35% in baseline and 92–94% in the blocking experiments, in cerebellum, putamen, and choroid plexus of the fourth ventricle, respectively. The effect of receptor blockade in brain was evident from the faster washout compared to baseline (Table II). Since brain receptors were blocked by nonradioactive ligand, the radiotracer was not significantly retained in brain.

What percentage of brain uptake was displaceable, i.e., specifically bound to PBRs? Specific binding can be estimated by comparing brain activity before and after blockade at later time points when the effects of blood flow are less prominent. In Figures 2 and 3, ~80 and 60% of total uptake were displaceable for [^{18}F]PBR06 and [^{11}C]PBR01, respectively. These values for specific binding are likely underestimations, since they did not correct for the higher plasma delivery to brain in the blocked condition. Although this simple empirical analysis of the brain curves showed that the majority of brain uptake of both [^{18}F]PBR06 and [^{11}C]PBR01 was displaceable, V from compartmental modeling will provide more accurate values, since they correct for brain uptake relative to the plasma delivery to brain.

[^{18}F]PBR06: compartmental analysis

Both one- and two-tissue compartment models converged in all regions with 5-h data (scans #3 and 4; Table I), but the fitting did not converge with only 2-h data (scan #1). The two-tissue compartment model provided significantly better fitting in all regions of the two baseline experiments (Fig. 2A). The MSC (AIC) values in all regions were 2.09 ± 0.50 (1437 ± 167) and 4.03 ± 0.50 (1334 ± 171) for the one- and two-tissue compartment models, respectively (Tables III and IV). The two-tissue compartment model identified V well with 2.8 ± 1.0% COV. Therefore, the two-tissue compartment model well described the kinetics of [^{18}F]PBR06 and provided reliable measurements of V. Averaged V values by two-tissue compartment model were 60, 80, and 78 mL/cm^3 in cerebellum, putamen, and choroid plexus of the fourth ventricle, respectively (Table IV).

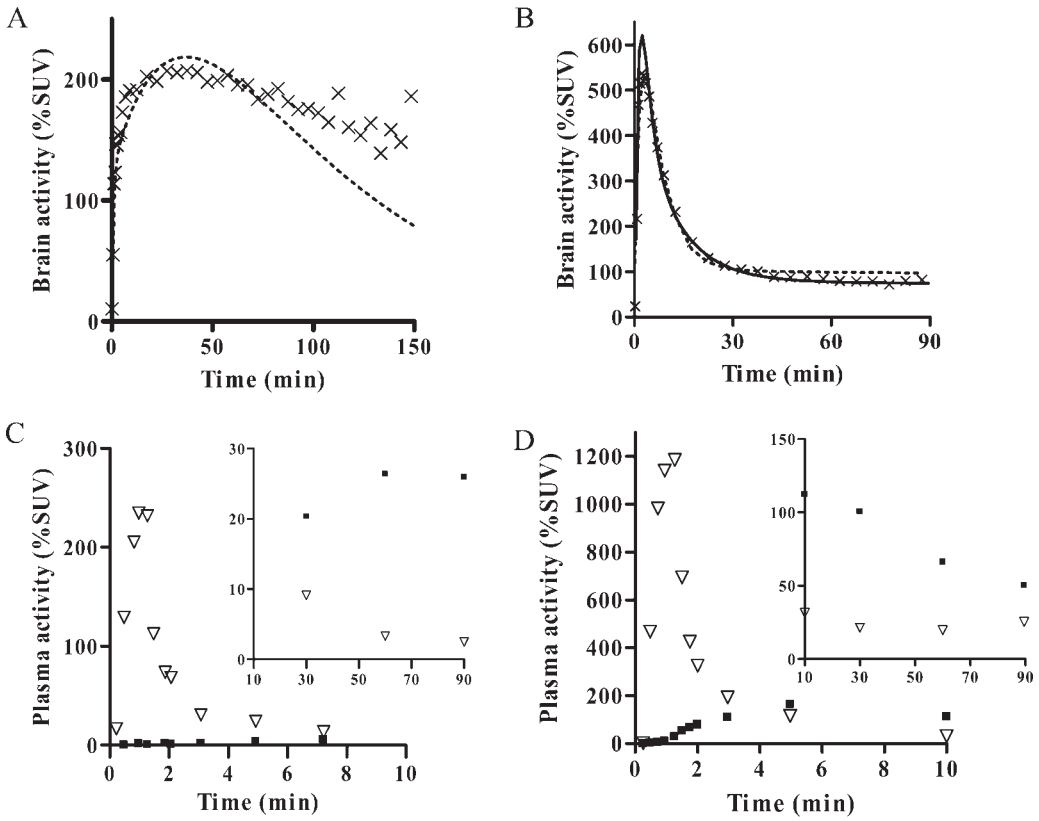

Fig. 3. Representative [^{11}C]PBR01 brain time-activity curves, compartmental fittings, and radioligand concentrations in plasma of baseline (**A** and **C**; scan #5, Table I) and after receptor blockade (**B** and **D**; scan #6, Table I). Nonradiolabeled PBR01 (1 mg/kg) was injected at the same time of [^{11}C]PBR01 injection in the blocking experiment. In the brain curves (A and B), the dashed line is the one-tissue compartment fitting, and the solid line is the two-tissue compartment fit. Two-tissue compartmental fitting did not converge in the baseline scan (A). For the plasma curves (C and D), the inset graphs show the lower plasma activities after 10 min. Symbols: (×) putamen, (▽) plasma parent, and (■) major radiometabolite.

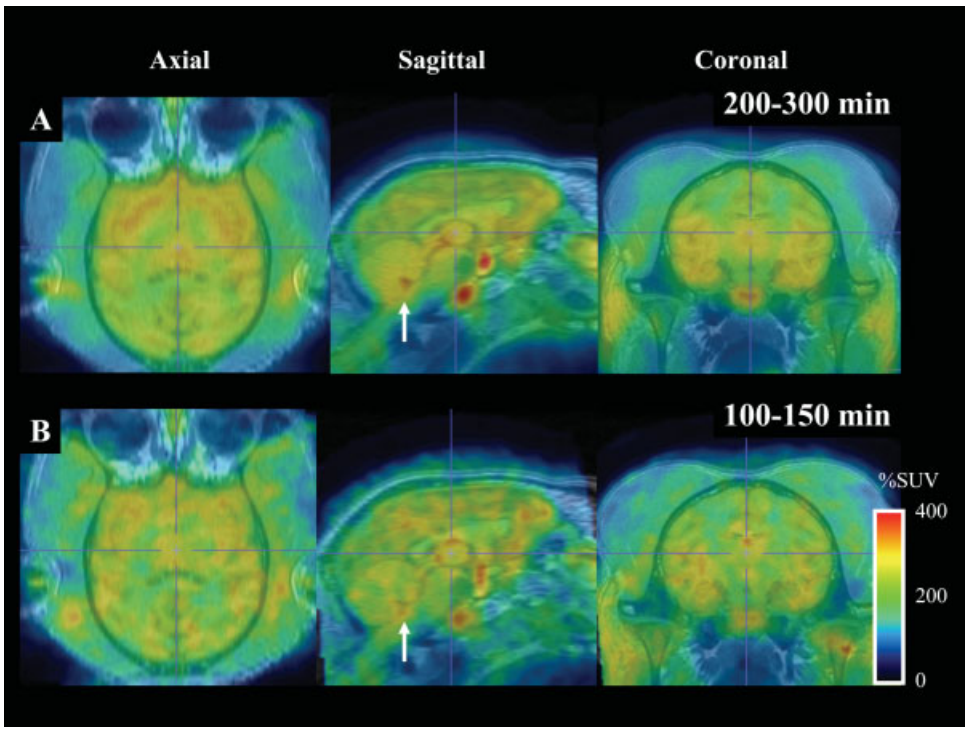

Fig. 4. PET averaged images at late time points for each PBR baseline scan: **A:** [^{18}F]PBR06 (200–300 min), scan #3 and **B:** [^{11}C]PBR01 (100–150 min), scan #7 in Table I. These images were created using averaged HRRT images at late time points in the same animal (#2). [^{11}C]PBR01 and [^{18}F]PBR06 showed high brain uptake (300% SUV) and widespread distribution in brain, which is consistent with known distribution of the receptor. The choroid plexus of the fourth ventricle (marked with arrow on sagittal images) had highest levels of activities within the skull. Activity is shown as %SUV, which normalizes for injected activity and body weight. %SUV = (% injected activity/cm^3 tissue) × body weight (g).

TABLE II. Averaged regional peak uptake times and regional activity washout rate

	[^{18}F]PBR06				[^{11}C]PBR01			
	Baseline ($N = 3$)		Blocking ($N = 1$)		Baseline ($N = 2$)		Blocking ($N = 2$)	
Region	Peak uptake (min)	Washout (%)	Peak uptake (min)	Washout (%)	Peak uptake (min)	Washout (%)	Peak uptake (min)	Washout (%)
Cerebellum	34	32	3	92	35	35	3	92
Putamen	43	20	2	94	40	18	3	92
Choroid plexus	31	24	2	94	26	31	3	94

Regional activity washout rate: percentage decrease from peak to 120 min.

TABLE III. Results of PBR baseline experiments by one-tissue compartment model

Ligand	Region	K_1 (mL cm^{-3} min^{-1})	k_2 (min^{-1})	V (mL cm^{-3})	MSC	AIC
[^{18}F]PBR06	Cerebellum	0.45 (5.7)	0.009 (6.0)	49 (3.5)	1.76	1463
	Putamen	0.45 (2.4)	0.007 (5.2)	65 (3.5)	1.97	1454
	Choroid plexus	0.55 (3.2)	0.009 (5.9)	62 (3.7)	1.30	1505
[^{11}C]PBR01	Cerebellum	0.46 (5.8)	0.019 (7.1)	24 (3.1)	2.32	875
	Putamen	0.37 (1.8)	0.012 (5.2)	30 (3.9)	2.25	863
	Choroid plexus	0.58 (2.5)	0.020 (5.4)	29 (3.6)	1.82	904

Numbers in parentheses indicate identifiably of rate constants expressed as %COV.
MSC, model selection criterion; AIC, akaike information criterion.

TABLE IV. Results of PBR baseline experiments by two-tissue compartment model

Ligand	Region	K_1 (mL cm^{-3} min^{-1})	k_2 (min^{-1})	k_3 (min^{-1})	k_4 (min^{-1})	V (mL cm^{-3})	MSC	AIC
[^{18}F]PBR06	Cerebellum	0.65 (7.2)	0.039 (16.1)	0.028 (14.7)	0.011 (6.5)	60 (2.2)	4.32	1329
	Putamen	0.67 (2.6)	0.044 (12.7)	0.043 (13.0)	0.009 (6.2)	80 (2.3)	4.21	1337
	Choroid plexus	0.87 (3.1)	0.049 (11.7)	0.033 (13.9)	0.009 (7.8)	78 (3.0)	3.36	1395
[^{11}C]PBR01	Cerebellum	0.58 (2.9)	0.067 (9.2)	0.048 (13.1)	0.011 (38.5)	66 (26.8)	4.35	499
	Putamen	0.46 (2.5)	0.068 (12.1)	0.072 (17.2)	0.008 (59.3)	92 (45.0)	3.63	512
	Choroid plexus	0.75 (2.6)	0.080 (9.8)	0.051 (15.6)	0.009 (64.7)	100 (49.5)	3.28	551

Numbers in parentheses indicate identifiably of rate constants expressed as %COV.
MSC, model selection criterion; AIC, akaike information criterion.
Results of one scan are shown for [^{11}C]PBR01, where the two-tissue compartment model converged.

In a blocking experiment (scan #2; Table I), the one-tissue compartment model fit poorly and had MSC (AIC) values of 2.57 ± 0.61 (725 ± 20). The two-tissue compartment model did not converge in some regions. Poor identifiability of k_4 likely caused the failure of convergence, since %COV of k_4 was as large as 18–104% in areas where the two-tissue compartment model fitting converged in the same experiment (Fig. 2B). V values by one-tissue compartment model were 2.0, 2.4, and 2.3 mL/cm^3 in cerebellum, putamen, and choroid plexus of the fourth ventricle, respectively.

By using V values obtained with two-tissue compartment model in baseline and with the one-tissue compartment model in blocking scans, ~97% of V in baseline scans was specific binding. However, this value was likely overestimated because of the underestimation of V values in the blocking scans.

Estimation of minimal scan length for [^{18}F]PBR06

To investigate the effect of reducing the scan duration on measurement of V, kinetic analysis was performed with scan durations ranging from 100 to 300 min for [^{18}F]PBR06, with 10–20 min increments. Values of V obtained with shortened data length were compared with that obtained with the 300-min data. Because the two-tissue compartment model well described the kinetics, it was used to estimate the minimal scan length for accurate measurement. After 200 min, V by two-tissue compartment model became independent of scan length in all regions. The results of the choroid plexus of the fourth ventricle are shown in Figure 5. Percentage differences in V obtained with shortened and full length data were within ±10% after 200 min in two baseline experiments in cerebellum, putamen, and choroid plexus of the fourth ventricle (scans #3 and 4). In these regions, the COV of V was also less than 10% after 200 min. Therefore, the value of V was stably and reliably determined with 200 min of scanning for [^{18}F]PBR06.

[^{11}C]PBR01: compartmental analysis

Although 200-min data acquisition was required for [^{18}F]PBR06, baseline data of [^{11}C]PBR01 was acquired for only ~150 min because of the short half-life of ^{11}C. As described below, similar to [^{11}C]PBR01, the one-tis-

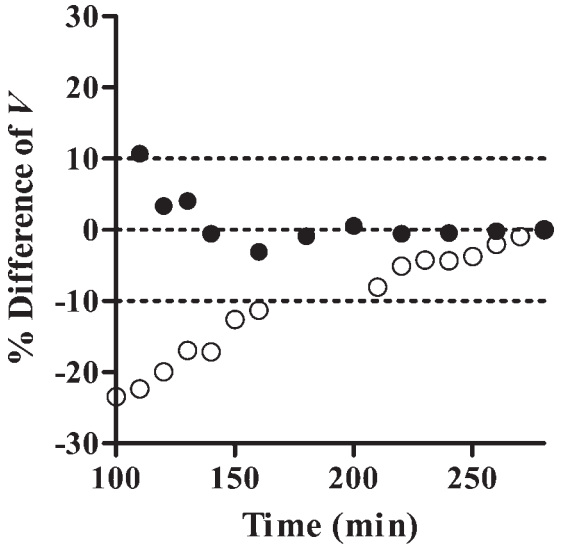

Fig. 5. Relationship between V of [^{18}F]PBR06 obtained by a two-tissue compartment model and the experiment duration in choroid plexus of the fourth ventricle. Baseline scans were analyzed using brain data from time zero to the specified time. For all baseline scans, 200 min imaging time provided V within ±10% of the values obtained with the full length data. % difference = $[(V_{exp} - V_{full})/V_{full}] \times 100$, where V_{exp} is the V determined from the shortened data and V_{full} is the V estimated from the full-length data. (○) #3 and (●) #4.

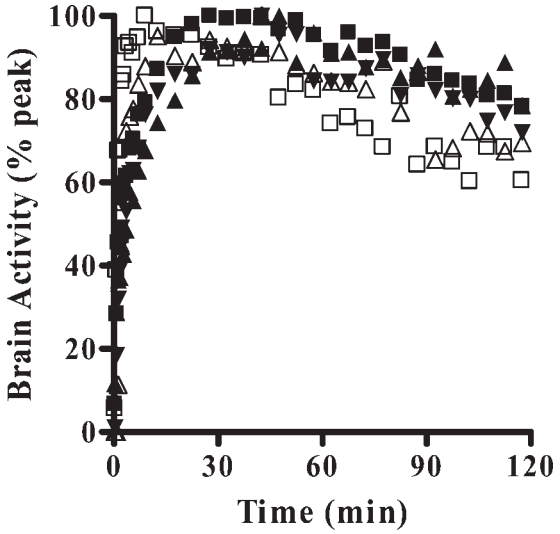

Fig. 6. Normalized brain activities in choroid plexus of the fourth ventricle for all baseline experiments of [^{18}F]PBR06 (solid symbols) and [^{11}C]PBR01 (open symbols). Brain activity was normalized to the peak value in each scan and plotted for the initial 120 min. Both [^{18}F]PBR06 and [^{11}C]PBR01 showed peak brain uptake in the choroid plexus at ~30 min, with 20–30% decrease of brain radioactivity between 30 and 120 min in all experiments. Scan #1 (■); #3 (▲); #4 (▼); #5 (□; #7 (△) (Table I).

sue compartment model did not provide good fitting. However, the two-tissue compartment model, for which longer data acquisition may be required to identify four parameters, did not converge. Therefore, this ligand did not provide accurate measurement of PBR binding.

In two baseline experiments (scans #5 and #7), the one-tissue compartment model converged with poor fitting and MSC (AIC) values of only 2.18 ± 1.00 (873 ± 98) (Fig. 3A). Average V values by one-tissue compartment model were 24, 30, and 29 mL/cm^3 with good identifiability of 3.1–3.9% COV in cerebellum, putamen, and choroid plexus of the fourth ventricle, respectively (Table III). In one of two baseline experiments (scan #5), the two-tissue compartment model did not converge in most regions. Poor identifiability of k_4 likely caused the lack of convergence, since %COV of k_4 was as large as 69–117% in areas where the two-tissue compartment fit worked well. Therefore, V of [^{11}C]PBR01 could not be measured accurately in baseline scans, because two-tissue compartment model did not converge in one experiment, and one-tissue compartment model apparently underestimated values at late time points (Fig. 3A).

In two blocking experiments (scans #6 and #8), both one- and two-tissue compartment models converged in all regions. One of two blocking experiments (scan #6) showed that two-tissue compartment model provided significantly better fitting than one-tissue compartment model (Fig. 3B). The MSC (AIC) values were 3.69 ± 0.30 (536 ± 10) and 6.02 ± 0.44 (473 ± 10) for the one- and two-tissue compartment models, respectively. Two-tissue compartment V values were 3.0, 3.3, and 3.4 mL/cm^3 with good identifiability of 0.9–1.0% COV in cerebellum, putamen, and choroid plexus of the fourth ventricle, respectively. In the other blocking scan, where one- and two-tissue compartment models showed similar goodness-of-fit, V values by these models were almost identical with the results of 1.3, 1.4, and 1.3 and 1.3, 1.4, and 1.4 mL/cm^3 with good identifiability of 1.9–6.5% COV in cerebellum, putamen, and choroid plexus of the fourth ventricle, respectively.

By comparing V measured with one-tissue compartment model in baseline and two-tissue compartment model in blocking scans, ~92% of total activity represented specific binding. However, this estimate was prone to error because of the poor fitting of one-tissue compartment model. In fact, the percentage of specific binding was likely underestimated because of the underestimation of V in the baseline scans.

Comparison of [^{11}C]PBR01 and [^{18}F]PBR06

The brain kinetics of these two ligands was quite similar, with the exception that the ^{18}F-tracer allowed longer scans than the ^{11}C-tracer. Both ligands showed peak brain uptake in the choroid plexus at ~30 min, with 20–30% decrease of brain radioactivity in the subsequent 90 min (Table II and Fig. 6). In addition, [^{18}F]PBR06 and [^{11}C]PBR01 showed similar plasma clearances and had average values of 1250 and 1010 mL/min, respectively.

To assess the effect of scan length on identifiability of V, we compared the two ligands using only the

initial 120 min of data for each. The one-tissue compartment model converged with poor fitting for both tracers and had average MSC (AIC) values of 2.49 (769) and 2.13 (798) for [^{18}F]PBR06 and [^{11}C]PBR01, respectively. In addition, most two-tissue compartmental fittings did not converge or showed significant errors compared to the results using 5-h data.

DISCUSSION

Using nonhuman primates, we performed an initial evaluation of two new PET PBR ligands that have an aryloxyanilide structure. For both [^{18}F]PBR06 and [^{11}C]PBR01, imaging with a receptor-blocking agent caused quick washout of activity from the brain indicating high levels of specific binding (Table II, Figs. 2B and 3B). Receptor blockade also caused a marked increase of the concentration of radiotracer in plasma, and analysis of only the brain curves would underestimate the percentage of specific binding. Thus, we estimate specific binding with *V*, which normalized brain uptake relative to the plasma concentration of radiotracer. Comparison of *V* in both baseline and blocked scans showed that as much as ~90% of total binding was specific for both [^{18}F]PBR06 and [^{11}C]PBR01 in nonhuman primate brain. *V* of [^{11}C]-PBR01 was inaccurately estimated in the baseline scans (Fig. 3A), possibly because of the short half-life of ^{11}C relative to ligand washout. On the other hand, *V* for [^{18}F]PBR06 showed good fitting (Fig. 2A) with high identifiability (Table III), and the estimates were independent of scan length after 200 min (Fig. 5). Therefore, [^{18}F]PBR06 is a promising ligand to detect changes in PBR in neuroinflammation and should be further tested in humans.

PBR has fairly uniform and widespread distribution in human brain as shown by in vitro autoradiography (Doble et al., 1987), but detailed distribution of PBR in nonhuman primate brain has not been reported with in vitro experiments. The current study in monkey brain showed widespread distribution of radioligand uptake (Fig. 4), which was displaced to uniform low levels of nonspecific and free radiotracer (Fig. 2B and 3B). In addition, both the current study (Fig. 4) and an in vitro experiment using [^{3}H]1-(2-chlorophenyl)-*N*-methyl-*N*-(1-methylpropy)-3-isoquinolinecarboxamide ([^{3}H]Ro5-4864) showed a high density PBR in the choroid plexus of rhesus monkey (Cymerman et al., 1986). Because of the widespread distribution of PBRs in brain and the absence of a large receptor-free region, we did not attempt to use reference tissue models.

We initiated the study with the GE Advance and subsequently acquired data with the higher resolution Siemens HRRT. We think that the use of two cameras did not confound the interpretation of the results for large ROIs, since both were calibrated relative to the same phantom. In addition, most comparisons between studies (e.g., baseline versus blocked) used the same device. Nevertheless, differences in resolution could affect quantitation of small targets like the choroid plexus of the fourth ventricle. Measured as the full-width at half maximum, the resolution of the GE Advance and HRRT is 7.5 and 2.5 mm, respectively. The results of the choroid plexus described earlier were obtained using ROIs with an average volume of 81 mm^3. To assess the effect of greater spatial resolution, images from both cameras were reanalyzed using smaller ROIs with an average volume of 16 mm^3. Even for this visually detectable smallest structure, the small and large ROIs gave similar values for the HRRT and GE Advance, with average differences of 1.9 and 1.7% in *V*, respectively. Thus, differences between cameras due to spatial resolution were small for all regions larger than the choroid plexus ROI. The density of [^{3}H]Ro5-4864 binding sites in monkey choroid plexus was 1.8-fold higher than that in cerebellum (Cymerman et al., 1986). On both cameras, the study showed slightly lower but similar ratios of ~1.3 in choroid plexus/cerebellum using *V* values of [^{18}F]PBR06 measured by the two-tissue compartment model (Table IV). The lower in vivo ratio may have been caused by nondisplaceable activity in the PET measurement and differences between in vitro and in vivo experimental conditions, including temperature and anesthesia.

[^{11}C]PBR01 did not provide accurate measurement of *V* because of poor fitting by the one-tissue compartment (Fig. 3A) and the failure of convergence by the two-tissue compartment model. The reasons for the poor fitting were unclear but could include the possible presence of radiometabolite in brain or slow dissociation of the radioligand from the receptor. In contrast, *V* of [^{18}F]PBR06 could be reliably quantified with the two-tissue compartment model. Furthermore, the two-tissue compartment model was significantly better than the one-tissue compartment fitting, indicating that the [^{18}F]PBR06 did not distribute instantaneously in all tissue compartments. Nevertheless, accurate quantification of nonspecific binding was complicated by the fact that the blockade caused a marked increase of the radiotracer in plasma (Fig. 2C and 2D). We used a one-tissue compartment model to quantify nondisplaceable uptake, i.e., nonspecific binding plus free radiotracer in brain. These results suggested that the nondisplaceable distribution volume of [^{18}F]PBR06 was extremely small (2.3 mL/cm^3 in choroid plexus; data not shown) compared to that the two-tissue compartment model in baseline condition (78 mL/cm^3 in choroid plexus; Table IV). We suspect the nondisplaceable distribution volume was underestimated because the fitted line was lower than the measured radioactivity values, especially at later time points (Fig. 2B). One potential reason for the somewhat poor fitting of the latter time points in the blocked state (Fig. 2B) would be the presence of radiometabolite in the brain. Although the radi-

oactive metabolites were relatively less lipophilic than the parent compounds but still with the ability to enter the brain, their plasma levels increased at later time points to constitute 70–80% of total plasma activity and might have entered the brain slowly over time.

We found that [^{18}F]PBR06 provided more accurate measurement of PBR than [^{11}C]PBR01, but we were able to image ^{18}F activity longer than ^{11}C. Thus, the superiority of [^{18}F]PBR06 relative to [^{11}C]PBR01 may have been because of the longer half-life of ^{18}F and not solely because of its chemical and pharmacological properties. In fact, both ligands showed similar clearance, time to peak of brain activities, and washout rates (Table II and Fig. 6). Moreover, by using 120-min data of both ligands, kinetics was not well described by one- and two-tissue compartment models compared to the results using 5-h data (Fig. 5). In other words, if both ligands were analyzed for the same period of time (120 min), they showed similar kinetics as well as comparable deficiencies with compartmental quantitation.

Two aryloxyanilide compounds, [^{11}C]DAA1106 and [^{18}F]FEDAA1106, were previously shown to label PBRs in monkey brain (Maeda et al., 2004; Zhang et al., 2004). The proportion of specific binding was not performed in same way that we did, i.e., compartmental modeling with arterial input to correct for displacement from peripheral sites. Nevertheless, these ligands appear to have similarly high proportion of specific binding based on displacement studies.

In conclusion, [^{18}F]PBR06 showed sufficient signal and appropriate kinetics to allow quantitative analysis of the total brain uptake (specific plus nondisplaceable radioactivity) with 200 min of imaging in nonhuman primate brain. The high proportion of specific relative to nonspecific binding should provide high sensitivity to detect small changes in PBRs in brain. Moreover, ^{18}F is more convenient than ^{11}C by allowing multiple injections from a single synthesis during the course of a day or shipment of the radiopharmaceutical to distant facilities.

ACKNOWLEDGMENTS

We thank Jeih-San Liow, PhD for processing PET data and PMOD Technologies for providing its image analysis and modeling software. In vitro receptor screening at all sites other than that labeled with [^{3}H]PK 11195 was performed by the NIMH's Psychoactive Drug Screening Program (Contract # NO1MH32004).

REFERENCES

Akaike H. 1974. A new look at the statistical model identification. IEEE Trans Automat Control AC 19:716–723.

Anholt RR, Murphy KM, Mack GE, Snyder SH. 1984. Peripheral-type benzodiazepine receptors in the central nervous system: Localization to olfactory nerves. J Neurosci 4:593–603.

Anholt RR, Pedersen PL, De Souza EB, Snyder SH. 1986. The peripheral-type benzodiazepine receptor. Localization to the mitochondrial outer membrane. J Biol Chem 261:576–583.

Banati RB. 2002. Visualising microglial activation in vivo. Glia 40:206–217.

Banati RB. 2003. Neuropathological imaging: In vivo detection of glial activation as a measure of disease and adaptive change in the brain. Br Med Bull 65:121–131.

Banati RB, Goerres GW, Myers R, Gunn RN, Turkheimer FE, Kreutzberg GW, Brooks DJ, Jones T, Duncan JS. 1999. [^{11}C](R)-PK11195 positron emission tomography imaging of activated microglia in vivo in Rasmussen's encephalitis. Neurology 53:2199–2203.

Banati RB, Newcombe J, Gunn RN, Cagnin A, Turkheimer F, Heppner F, Price G, Wegner F, Giovannoni G, Miller DH, Perkin GD, Smith T, Hewson AK, Bydder G, Kreutzberg GW, Jones T, Cuzner ML, Myers R. 2000. The peripheral benzodiazepine binding site in the brain in multiple sclerosis: Quantitative in vivo imaging of microglia as a measure of disease activity. Brain 123 (Part 11):2321–2337.

Benavides J, Quarteronet D, Imbault F, Malgouris C, Uzan A, Renault C, Dubroeucq MC, Gueremy C, Le Fur G. 1983. Labelling of "peripheral-type" benzodiazepine binding sites in the rat brain by using [^{3}H]PK 11195, an isoquinoline carboxamide derivative: Kinetic studies and autoradiographic localization. J Neurochem 41:1744–1750.

Benavides J, Fage D, Carter C, Scatton B. 1987. Peripheral type benzodiazepine binding sites are a sensitive indirect index of neuronal damage. Brain Res 421:167–172.

Bevington PR,Robinson DL, editor. 2003. Data reduction and error analysis for the physical sciences. New York: McGraw-Hill.

Bono F, Lamarche I, Prabonnaud V, Le Fur G, Herbert JM. 1999. Peripheral benzodiazepine receptor agonists exhibit potent antiapoptotic activities. Biochem Biophys Res Commun 265:457–461.

Briard E, Hong J, Musachio JL, Zoghbi SS, Fujita M, Imaizumi M, Cropley V, Innis RB, Pike VW. 2005a. Synthesis and evaluation of two candidate ^{11}C-labeled radioligands for brain peripheral benzodiazepine receptors. J Label Compd Radiopharm 48:S71.

Briard E, Shah J, Musachio JL, Zoghbi SS, Fujita M, Imaizumi M, Cropley V, Innis RB, Pike VW. 2005b. Synthesis and evaluation of a new ^{18}F-labeled ligand for PET imaging of brain peripheral benzodiazepine receptors. J Label Compd Radiopharm 48:S4.

Burger C, Mikolajczyk K, Grodzki M, Rudnicki P, Szabatin M, Buck A. 1998. JAVA tools quantitative post-processing of brain PET data. J Nucl Med 39:277P.

Cagnin A, Brooks DJ, Kennedy AM, Gunn RN, Myers R, Turkheimer FE, Jones T, Banati RB. 2001a. In-vivo measurement of activated microglia in dementia. Lancet 358:461–467.

Cagnin A, Myers R, Gunn RN, Lawrence AD, Stevens T, Kreutzberg GW, Jones T, Banati RB. 2001b. In vivo visualization of activated glia by [^{11}C] (R)-PK11195-PET following herpes encephalitis reveals projected neuronal damage beyond the primary focal lesion. Brain 124 (Part 10):2014–2027.

Cagnin A, Gerhard A, Banati RB. 2002. In vivo imaging of neuroinflammation. Eur Neuropsychopharmacol 12:581–586.

Carson R. 1986. Positron emission tomography and Autoradiography: Principles and Applications from the Brain and Heart. In: Phelps ME MJ, Schelbert HR, editor. Parametric estimation in positron emission tomography. New York: Raven Press. p 347–390.

Chaki S, Funakoshi T, Yoshikawa R, Okuyama S, Okubo T, Nakazato A, Nagamine M, Tomisawa K. 1999. Binding characteristics of [^{3}H]DAA1106, a novel and selective ligand for peripheral benzodiazepine receptors. Eur J Pharmacol 371:197–204.

Cheng Y, Prusoff WH. 1973. Relationship between the inhibition constant (K1) and the concentration of inhibitor which causes 50 per cent inhibition (I50) of an enzymatic reaction. Biochem Pharmacol 22:3099–3108.

Cunningham VL, AA. 1995. Radioligand studies in brain: Kinetic analysis of PET data. Med Chem Res 5:79–96.

Cymerman U, Pazos A, Palacios JM. 1986. Evidence for species differences in "peripheral" benzodiazepine receptors: An autoradiographic study. Neurosci Lett 66:153–158.

Debruyne JC, Versijpt J, Van Laere KJ, De Vos F, Keppens J, Strijckmans K, Achten E, Slegers G, Dierckx RA, Korf J, De Reuck JL. 2003. PET visualization of microglia in multiple sclerosis patients using [^{11}C]PK11195. Eur J Neurol 10:257–264.

Doble A, Malgouris C, Daniel M, Daniel N, Imbault F, Basbaum A, Uzan A, Gueremy C, Le Fur G. 1987. Labelling of peripheral-type benzodiazepine binding sites in human brain with [^{3}H]PK 11195: Anatomical and subcellular distribution. Brain Res Bull 18:49–61.

Fujimura Y, Ikoma Y, Yasuno F, Suhara T, Ota M, Matsumoto R, Nozaki S, Takano A, Kosaka J, Zhang MR, Nakao R, Suzuki K, Kato N, Ito H. 2006. Quantitative analyses of ^{18}F-FEDAA1106

binding to peripheral benzodiazepine receptors in living human brain. J Nucl Med 47:43–50.
Gerhard A, Banati RB, Goerres GB, Cagnin A, Myers R, Gunn RN, Turkheimer F, Good CD, Mathias CJ, Quinn N, Schwarz J, Brooks DJ. 2003. [^{11}C](R)-PK11195 PET imaging of microglial activation in multiple system atrophy. Neurology 61:686–689.
Groom GN, Junck L, Foster NL, Frey KA, Kuhl DE. 1995. PET of peripheral benzodiazepine binding sites in the microgliosis of Alzheimer's disease. J Nucl Med 36:2207–2210.
Hawkins RA, Phelps ME, Huang SC. 1986. Effects of temporal sampling, glucose metabolic rates, and disruptions of the blood-brain barrier on the FDG model with and without a vascular compartment: Studies in human brain tumors with PET. J Cereb Blood Flow Metab 6:170–183.
Maeda J, Suhara T, Zhang MR, Okauchi T, Yasuno F, Ikoma Y, Inaji M, Nagai Y, Takano A, Obayashi S, Suzuki K. 2004. Novel peripheral benzodiazepine receptor ligand [^{11}C]DAA1106 for PET: An imaging tool for glial cells in the brain. Synapse 52:283–291.
McEnery MW, Snowman AM, Trifiletti RR, Snyder SH. 1992. Isolation of the mitochondrial benzodiazepine receptor: Association with the voltage-dependent anion channel and the adenine nucleotide carrier. Proc Natl Acad Sci USA 89:3170–3174.
Okubo T, Yoshikawa R, Chaki S, Okuyama S, Nakazato A. 2004. Design, synthesis and structure-affinity relationships of aryloxyanilide derivatives as novel peripheral benzodiazepine receptor ligands. Bioorg Med Chem 12:423–438.
Okuyama S, Chaki S, Yoshikawa R, Ogawa S, Suzuki Y, Okubo T, Nakazato A, Nagamine M, Tomisawa K. 1999. Neuropharmacological profile of peripheral benzodiazepine receptor agonists, DAA1097 and DAA1106. Life Sci 64:1455–1464.
Ouchi Y, Yoshikawa E, Sekine Y, Futatsubashi M, Kanno T, Ogusu T, Torizuka T. 2005. Microglial activation and dopamine terminal loss in early Parkinson's disease. Ann Neurol 57:168–175.
Papadopoulos V, Amri H, Boujrad N, Cascio C, Culty M, Garnier M, Hardwick M, Li H, Vidic B, Brown AS, Reversa JL, Bernassau JM, Drieu K. 1997. Peripheral benzodiazepine receptor in cholesterol transport and steroidogenesis. Steroids 62:21–28.
Petit-Taboue MC, Baron JC, Barre L, Travere JM, Speckel D, Camsonne R, MacKenzie ET. 1991. Brain kinetics and specific binding of [^{11}C]PK 11195 to omega 3 sites in baboons: Positron emission tomography study. Eur J Pharmacol 200:347–351.
Price CJ, Wang D, Menon DK, Guadagno JV, Cleij M, Fryer T, Aigbirhio F, Baron JC, Warburton EA. 2006. Intrinsic activated microglia map to the peri-infarct zone in the subacute phase of ischemic stroke. Stroke 37:1749–1753.
Schlichter R, Rybalchenko V, Poisbeau P, Verleye M, Gillardin J. 2000. Modulation of GABAergic synaptic transmission by the non-benzodiazepine anxiolytic etifoxine. Neuropharmacology 39:1523–1535.
Schoemaker H, Boles RG, Horst WD, Yamamura HI. 1983. Specific high-affinity binding sites for [^{3}H]Ro 5–4864 in rat brain and kidney. J Pharmacol Exp Ther 225:61–69.
Turner MR, Cagnin A, Turkheimer FE, Miller CC, Shaw CE, Brooks DJ, Leigh PN, Banati RB. 2004. Evidence of widespread cerebral microglial activation in amyotrophic lateral sclerosis: An [^{11}C](R)-PK11195 positron emission tomography study. Neurobiol Dis 15:601–609.
Zavala F. 1997. Benzodiazepines, anxiety and immunity. Pharmacol Ther 75:199–216.
Zhang MR, Kida T, Noguchi J, Furutsuka K, Maeda J, Suhara T, Suzuki K. 2003. [^{11}C]DAA1106: Radiosynthesis and in vivo binding to peripheral benzodiazepine receptors in mouse brain. Nucl Med Biol 30:513–519.
Zhang MR, Maeda J, Ogawa M, Noguchi J, Ito T, Yoshida Y, Okauchi T, Obayashi S, Suhara T, Suzuki K. 2004. Development of a new radioligand, *N*-(5-fluoro-2-phenoxyphenyl)-N-(2-[^{18}F]fluoroethyl-5-methoxybenzyl)acetami de, for pet imaging of peripheral benzodiazepine receptor in primate brain. J Med Chem 47:2228–2235.
Zoghbi SS, Shetty HU, Ichise M, Fujita M, Imaizumi M, Liow JS, Shah J, Musachio JL, Pike VW, Innis RB. 2006. PET imaging of the dopamine transporter with ^{18}F-FECNT: A polar radiometabolite confounds brain radioligand measurements. J Nucl Med 47: 520–527.